

Unsupervised energy disaggregation via convolutional sparse coding

Christian Aarset, Andreas Habring, Martin Holler, Mario Mitter *

July 21, 2022

Abstract

In this work, a method for unsupervised energy disaggregation in private households equipped with smart meters is proposed. This method aims to classify power consumption as *active* or *passive*, granting the ability to report on the residents' activity and presence without direct interaction. This lays the foundation for applications like non-intrusive health monitoring of private homes.

The proposed method is based on minimizing a suitable energy functional, for which the iPALM (inertial proximal alternating linearized minimization) algorithm is employed, demonstrating that various conditions guaranteeing convergence are satisfied.

In order to confirm feasibility of the proposed method, experiments on semi-synthetic test data sets and a comparison to existing, supervised methods are provided.

1 Introduction

Smart meters – energy meters capable of digital communication – are becoming increasingly available in European domestic households. *Intelligente Messgeräte-Einführungsverordnung – IME-VO* [2] derived from the EU directive [1] dictates that 95% of all Austrian meter points have to be equipped with smart meters by the end of 2024.

As a result, regular readings of household energy consumption will be available on a large scale, potentially enabling a variety of insights into power consumption, usage patterns and human activity. For an overview of possible health care applications of smart meters see [9,22]. Motivated by the possibility of automatically detecting emergencies and health issues from anomalous human activity or from lack of activity, we focus on the latter in this work. Such an automatic detection would alleviate the need for the consumer to report incidents manually,

and would bypass the usage of intrusive surveillance devices.

Smart meters measure the aggregate energy consumption of a household rather than the consumptions of individual devices. Obtaining detailed information about the composition of the aggregate data is difficult, as it requires either directly measuring the energy consumption at many different points in the electrical circuit, potentially demanding costly installations, or computational separation of the smart meter signal into distinct contributions, which is inherently ill-posed. Despite this, there exists a variety of methods for *energy disaggregation*, also referred to as *non-intrusive load monitoring* (NILM), that is, recovering the individual device power consumptions from the aggregated data. A recent review of existing methods for NILM can be found in [10].

Broadly speaking, one might categorise such disaggregation methods as *supervised*, meaning labeled training data is available, or *unsupervised* in the converse case. While the latter case is substantially more difficult, it is also more relevant for practical applications, due to the cost and difficulty of collecting data on a representative household sample. One of the first approaches introduced in [11] is based on matching the changes in power consumption to certain devices in the household. Many works propose the use of different versions of hidden Markov models [3, 12, 15, 18, 21]. While these can, in principle, also be used as *unsupervised* methods, it should be mentioned that estimating the necessary parameters requires either strong assumptions or significant prior knowledge about the devices. In [17, 20], the authors propose sparse coding for NILM, and in [24], this approach is extended to a deep sparse coding model. More recently, deep learning methods have also been applied to NILM, c.f. [13, 19, 25, 26].

In this work, we propose a sparse coding approach similar to [17, 20]. Contrary to these works, however, our method completely omits any prior dictionary learning using labeled data. This approach increases robustness when little or no ground truth is available. Motivated by the aforementioned monitoring applications, we will provide experimental results for the simpler problem of activity prediction as well as for

*The SOLGENIUM Project: Supported by the Austrian Research Promotion Agency (FFG) (Grant 881561).

full disaggregation into individual devices. For activity prediction, we disaggregate into an *active* and a *passive channel*, where the presence of the former will be used as an indicator of human activity.

1.1 Discrete convolutions

The fundamental observation motivating our approach is that the main contributors to a household's energy consumption consist of disparate device power consumption peaks, or simply *device characteristics*. That is, whenever a device is used for a fixed period of time, the graph tracking its individual power consumption over time will consistently be of the same approximate shape and magnitude. Moreover, most individual devices, in particular those corresponding to human activity, will be used sparsely, in the sense that the number of times they are activated and deactivated each day is relatively low, leading to a natural separation of incidents of each device characteristic on the temporal axis.

Inspired by this, we attempt to model the energy consumption graph by splitting it into several *channels*, each a graph of the same length that represents all occurrences of one device characteristic, or the collection of several similar device characteristics. In the application of activity detection, we will be particularly interested in the case where we have one *active channel*, representing the sum of the characteristics of all devices that require human interaction to enable – thus indicating human activity – and one *passive channel*, consisting of the characteristics of all remaining devices. Examples of devices contributing to the active channel include, but are not limited to, ovens, washing machines and hair dryers, while devices such as fridges and routers might contribute to the passive channel.

Explicitly, this leads to the following setting: With $m \in \mathbb{N}$, consider the energy consumption graph $u \in \mathbb{R}^m$. Given a channel of u , we seek to model each of its – potentially multiple – component characteristics as convolutions of *atoms* in \mathbb{R}^{2q+1} , $q \in \mathbb{N}$, and *coefficients* in \mathbb{R}^{m+2q} . This corresponds to the above notion that each channel consists of similar device characteristics, being approximated by the atom, and repeated on the temporal axis, that is, placed by the coefficients.

To enable this, define the convolution $*$: $\mathbb{R}^{m+2q} \times \mathbb{R}^{2q+1} \rightarrow \mathbb{R}^m$ via

$$\tilde{c} * \tilde{p} := \left(\sum_{\Delta q=-q}^q \tilde{c}_{j+q+\Delta q} \tilde{p}_{q+1-\Delta q} \right)_{j=1}^m \in \mathbb{R}^m.$$

Generally, we shall work with multiple coefficient-atom pairs, each atom p^i corresponding to one device characteristic and

the matching coefficient c^i corresponding to its placement in time. Given $N \in \mathbb{N}$ such coefficient-atom pairs $(c, p) = ((c^i)_{i=1}^N, (p^i)_{i=1}^N)$, we abuse notation and denote also by $*$: $(\mathbb{R}^{m+2q})^N \times (\mathbb{R}^{2q+1})^N \rightarrow \mathbb{R}^m$ the sum-of-convolutions map

$$c * p := \sum_{i=1}^N c^i * p^i.$$

We desire the following properties for our atoms and coefficients:

- The atoms should be bounded, so that amplitude scaling is left to the coefficients.
- Atoms and coefficients should be positive, as we do not currently account for energy-producing devices such as solar panels.
- With (c^1, p^1) representing the passive channel, we let all remaining pairs, that is, (c^i, p^i) for $i \geq 2$, serve to explain the active channel, in the sense that the active channel is approximated by $\sum_{i=2}^N c^i * p^i$. The coefficients c^i will be penalized in $\|\cdot\|_1$ -norm, emulating the previously mentioned temporal sparsity. However, we only penalize c^1 in $\|\cdot\|_2$ -norm, as some passive devices, such as a router, may consume power throughout most of the day.

Combining the above leads to the minimization problem

$$\begin{aligned} \min_{c, p} & \|u - c * p\|_2^2 + \lambda_p \|c^1\|_2 + \lambda_a \sum_{i=2}^N \|c^i\|_1 \\ \text{s.t. } & c \geq 0, p \geq 0, \|p^i\|_2 \leq 1 \text{ for all } i = 1, \dots, N, \end{aligned} \quad (1)$$

with $\lambda_p, \lambda_a > 0$; the positivity constraints $c \geq 0$ and $p \geq 0$ are meant in the componentwise sense.

2 iPALM

As (1) does not generally allow for an analytical solution, we require an appropriate algorithm to numerically solve the minimization problem. In that respect, we face two main difficulties with our problem formulation: It is neither jointly convex nor differentiable in (c, p) , meaning standard convex or gradient descent-based algorithms cannot be used as-is. To overcome this, we employ the inertial Proximal Alternating Linearized Minimization (iPALM) algorithm as proposed in [23], which is suitable for nonconvex, nonsmooth optimization problems of a particular structure. Therefore, we first rewrite

(1) into a form where the iPALM algorithm is applicable, i.e., we consider

$$\min_{c,p} F(c,p), \text{ where } F(c,p) := R(c,p) + f_1(c) + f_2(p). \quad (2)$$

Here, $R(c,p) := \|u - c * p\|_2^2$,

$$f_1(c) := \begin{cases} \lambda_p \|c^1\|_2 + \lambda_a \sum_{i=2}^N \|c^i\|_1, & c \geq 0, \\ \infty, & \text{otherwise,} \end{cases}$$

$$f_2(p) := \begin{cases} 0, & p \geq 0 \text{ and } \max_{1 \leq i \leq N} \|p^i\|_2 \leq 1, \\ \infty, & \text{otherwise.} \end{cases}$$

To ensure convergence of iPALM according to [23], several properties of the functionals involved in (2) need to be satisfied. It is clear that f_1 , f_2 and R are proper, lower semi-continuous, bounded from below, and that R is differentiable. Moreover, f_1 and f_2 are both convex, with f_1 being a linear combination of componentwise norms under a convex constraint, and f_2 simply being a convex constraint. We further need Lipschitz continuity of the derivative of R as stated in the following proposition.

Proposition 1. *For R as above, the following holds:*

1. *For any fixed $p \in (\mathbb{R}^{2q+1})^N$, $c \mapsto \nabla_c R(c,p)$ is Lipschitz continuous. Similarly, for any fixed $c \in (\mathbb{R}^{m+2q})^N$, $p \mapsto \nabla_p R(c,p)$ is Lipschitz continuous.*
2. *∇R is Lipschitz continuous on bounded subsets of $(\mathbb{R}^{m+2q})^N \times (\mathbb{R}^{2q+1})^N$.*

Proof. Write $R(c,p) := \|\cdot\|^2 \circ [u - \cdot] \circ (c * p)$. As the map $c \mapsto c * p$ is linear for fixed p , one has $c * p = P(p)c$ with $P : (\mathbb{R}^{2q+1})^N \rightarrow \mathbb{R}^{m \times N(m+2q)}$. Simultaneously, for fixed c , $c * p = C(c)p$ with $C : (\mathbb{R}^{m+2q})^N \rightarrow \mathbb{R}^{m \times N(2q+1)}$. Thus,

$$\nabla_c R(c,p) = -2P(p)^T [u - c * p],$$

$$\nabla_p R(c,p) = -2C(c)^T [u - c * p].$$

Explicitly, one can write $P(p)c = \sum_{i=1}^N P^i(p^i)c^i$, where

$$P^i(p^i) = \begin{bmatrix} p_{2q+1}^i & \cdots & p_1^i & 0 & \cdots & 0 \\ 0 & p_{2q+1}^i & \ddots & p_1^i & \cdots & \vdots \\ \vdots & \ddots & \ddots & \ddots & \ddots & 0 \\ 0 & \cdots & 0 & p_{2q+1}^i & \cdots & p_1^i \end{bmatrix}.$$

Consider that each $v \in (\mathbb{R}^{m+2q})^N$ with $\|v\|_2 = 1$ can be written in the form $v = [a_1 v^1 \dots a_N v^N]^T$, with $\|v^i\|_2 = 1$ for all i and $\sum_{i=1}^N a_i^2 = 1$. Now Cauchy-Schwarz's inequality yields

$$\|P(p)v\|_2 = \left\| \sum_{i=1}^N a_i P^i(p^i) v^i \right\|_2 \leq \sum_{i=1}^N |a_i| \|P^i(p^i)\|$$

$$\leq \sqrt{\sum_{i=1}^N a_i^2} \sqrt{\sum_{i=1}^N \|P^i(p^i)\|^2} = \sqrt{\sum_{i=1}^N \|P^i(p^i)\|^2},$$

which cannot generally be improved. In the same manner, one has $C(c)p = \sum_{i=1}^N C^i(c^i)p^i$, where

$$C^i(c^i) = \begin{bmatrix} c_{2q+1}^i & c_{2q}^i & \cdots & c_2^i & c_1^i \\ c_{2q+2}^i & c_{2q+1}^i & \cdots & c_3^i & c_2^i \\ \vdots & \vdots & \ddots & \vdots & \vdots \\ c_{m+2q-1}^i & c_{m+2q-2}^i & \cdots & c_m^i & c_{m-1}^i \\ c_{m+2q}^i & c_{m+2q-1}^i & \cdots & c_{m+1}^i & c_m^i \end{bmatrix}$$

and thus $\|C(c)\| \leq \sqrt{\sum_{i=1}^N \|C^i(c^i)\|^2}$.

It follows that for any fixed $p \in (\mathbb{R}^{2q+1})^N$ and any $c, \tilde{c} \in (\mathbb{R}^{m+2q})^N$, one has

$$\|\nabla_c R(c,p) - \nabla_c R(\tilde{c},p)\|_2 = 2\|P(p)^T[(\tilde{c} - c) * p]\|_2$$

$$= 2\|P(p)^T P(p)(\tilde{c} - c)\|_2 \leq 2\|P(p)\|^2 \|c - \tilde{c}\|_2$$

$$\leq 2 \left(\sum_{i=1}^N \|P^i(p^i)\|^2 \right) \|c - \tilde{c}\|_2 =: L_1(p) \|c - \tilde{c}\|_2 \quad (3)$$

and analogously, for all $c \in (\mathbb{R}^{m+2q})^N$ and all $p, \tilde{p} \in (\mathbb{R}^{2q+1})^N$,

$$\|\nabla_p R(c,p) - \nabla_p R(c,\tilde{p})\|_2 = 2\|C(c)^T[c * (\tilde{p} - p)]\|_2$$

$$= 2\|C(c)^T C(c)(\tilde{p} - p)\|_2 \leq 2\|C(c)\|^2 \|p - \tilde{p}\|_2$$

$$\leq 2 \left(\sum_{i=1}^N \|C^i(c^i)\|^2 \right) \|p - \tilde{p}\|_2 =: L_2(c) \|p - \tilde{p}\|_2, \quad (4)$$

showing 1).

To show 2), we note that as the maps $p \mapsto P(p)$, $p \mapsto P(p)^T$, $c \mapsto C(c)$ and $c \mapsto C(c)^T$ are linear and bounded, it is clear that $\nabla_c R(c,p)$ and $\nabla_p R(c,p)$ are differentiable with respect to (c,p) jointly, with bounded derivatives on bounded subsets of $(\mathbb{R}^{m+2q})^N \times (\mathbb{R}^{2q+1})^N$. The mean value inequality immediately yields Lipschitz continuity on bounded sets. \square

Remark 1. *The preceding theorem ensures that Assumption A of [23] is satisfied (note that the lower bound in condition*

(iv) of this assumption can be easily satisfied by choosing sub-optimal Lipschitz constants that are bounded from below by a positive number). Further, using results from [7], it is clear that the objective function in (2) is semi-algebraic; it thus satisfies the Kurdyka-Łojasiewicz property. Hence, under suitable upper bounds on the stepsizes (see Assumption B of [23]), the iPALM algorithm can be applied to (2), and it is guaranteed that any bounded sequence of iterates converges to a critical point of (2) ([23, Theorem 4.1]).

Remark 2. The Lipschitz constants from 1) in Proposition 1 are needed for the stepsize choice in the iPALM algorithm. Although the norms $\|P^i(p^i)\|$ resp. $\|C^i(c^i)\|$ can be computed as $\sqrt{\rho(P^i(p^i)^T P^i(p^i))}$ resp. $\sqrt{\rho(C^i(c^i)^T C^i(c^i))}$, with $\rho(\cdot)$ the spectral radius, this may prove impractical for numerics. Norm estimates on the $P^i(p^i)$ can be obtained as follows: With $J : \mathbb{R}^{m+2q} \rightarrow \ell^2(\mathbb{R})$, $(Jx)_i := x_i$ for $1 \leq i \leq m+2q$ and $(Jx)_i := 0$ otherwise, with $K : \mathbb{R}^{2q+1} \rightarrow \ell^1(\mathbb{R})$, $(Kx)_i := x_{i+2q+1}$ for $-2q \leq i \leq 0$ and $(Kx)_i := 0$ otherwise, and with $\tilde{*}$ the discrete convolution between $\ell^2(\mathbb{R})$ and $\ell^1(\mathbb{R})$, Young's inequality implies

$$\begin{aligned} \|P^i(p^i)c^i\|_2 &= \|c^i * p^i\|_2 \leq \|Jc^i \tilde{*} Kp^i\|_{\ell^2} \\ &\leq \|Jc^i\|_{\ell^2} \|Kp^i\|_{\ell^1} = \|c^i\|_2 \|p^i\|_1. \end{aligned}$$

Taking the supremum yields $\|P^i(p^i)\| \leq \|p^i\|_1$. A similar argument shows $\|C^i(c^i)\| \leq \|c^i\|_1$. Applying standard matrix norm estimates, one altogether has

$$\begin{aligned} \|C^i(c^i)\| &\leq \min \left\{ \|c^i\|_1, \sqrt{2q+1} \max_{0 \leq \Delta j \leq 2q} \sum_{j=1}^m c_{j+\Delta j}^i, \right. \\ &\quad \left. \sqrt{m} \max_{0 \leq \Delta j \leq m-1} \sum_{j=1}^{2q+1} c_{j+\Delta j}^i, \left(\sum_{j=1}^m \sum_{\Delta j=0}^{2q} |c_{j+\Delta j}^i|^2 \right)^{\frac{1}{2}} \right\}, \end{aligned}$$

where it can be seen that each of these estimates may be optimal under various circumstances. Note also that although similar estimates are available for $P^i(p^i)$, its particular structure causes these to all be bounded below by $\|p^i\|_1$.

Applied to our setting, the iPALM algorithm takes the following form: Fix a suitable non-zero initialisation $(c_{-1}, p_{-1}) = (c_0, p_0) \in (\mathbb{R}^{m+2q})^N \times (\mathbb{R}^{2q+1})^N$, all non-negative componentwise. Fix $\varepsilon \in (0, 1)$ small, and for $i \in \{1, 2\}$, choose $\bar{\alpha}_i \in (0, 1 - \varepsilon)$, $\bar{\beta}_i > 0$ arbitrary. Define $\gamma_i := \frac{\bar{\alpha}_i + 2\bar{\beta}_i}{2(1 - \varepsilon - \bar{\alpha}_i)} \lambda_i^+$, where λ_1^+ resp. λ_2^+ corresponds to the upper bound over all k on $L_1(p_k)$ as in (3), resp. $L_2(c_k)$ as in (4); when such a bound is not analytically apparent, a viable

substitute in the k -th iteration step is $\max_{1 \leq j \leq k} L_1(p_j)$ resp. $\max_{1 \leq j \leq k+1} L_2(c_j)$, possibly dropping early indices to avoid excessive size. For each $k \in \mathbb{N}_0$, repeat the following process:

Require: Pick $\alpha_1^k \in [0, \bar{\alpha}_1]$, $\beta_1^k \in [0, \bar{\beta}_1]$.

$$y_1^k := c_k + \alpha_1^k (c_k - c_{k-1})$$

$$z_1^k := c_k + \beta_1^k (c_k - c_{k-1})$$

$$\tau_1^k := \frac{(1+\varepsilon)\gamma_1 + (1+\beta_1^k)L_1(p_k)}{2 - \alpha_1^k}$$

$$c_{k+1} \in \text{prox}_{\tau_1^k}^{f_1} \left(y_1^k - \frac{1}{\tau_1^k} \nabla_{c_k} R(z_1^k, p_k) \right)$$

Require: Pick $\alpha_2^k \in [0, \bar{\alpha}_2]$, $\beta_2^k \in [0, \bar{\beta}_2]$.

$$y_2^k := p_k + \alpha_2^k (p_k - p_{k-1})$$

$$z_2^k := p_k + \beta_2^k (p_k - p_{k-1})$$

$$\tau_2^k := \frac{(1+\varepsilon)\gamma_2 + (1+\beta_2^k)L_2(c_{k+1})}{2 - \alpha_2^k}$$

$$p_{k+1} \in \text{prox}_{\tau_2^k}^{f_2} \left(y_2^k - \frac{1}{\tau_2^k} \nabla_p R(c_{k+1}, z_2^k) \right)$$

The mappings $\text{prox}_{\tau_1^k}^{f_1}$ and $\text{prox}_{\tau_2^k}^{f_2}$ above are proximal mappings (see [6, Chapter 6]), which are given explicitly as follows.

Proposition 2. For $t > 0$, the functions f_1, f_2 as above satisfy

$$(\text{prox}_t^{f_1}(c))^i = \begin{cases} \left(1 - \frac{\lambda_p/t}{\max\{\|c^1\|_1, \lambda_p/t\}} \right) [c^1]_+, & i = 1, \\ \left[c^i - \frac{\lambda_a}{t} \right]_+, & i > 1, \end{cases}$$

$$(\text{prox}_t^{f_2}(p))^i = \frac{[p^i]_+}{\max\{\|[p^i]_+\|_2, 1\}},$$

where $[\cdot]_+, |\cdot|, -$ and sign are understood componentwise.

Proof. Denote for any set E by δ_E the indicator function satisfying $\delta_E(x) = 0$ for $x \in E$ and $\delta_E(x) = \infty$ for $x \notin E$, and by δ_+ the indicators for the positive cones. P_E denotes projection onto E .

We begin by noting that [6, Theorem 6.6], and the fact that f_1 and f_2 can both be written as componentwise sums enables us to compute each proximal mapping componentwise, with the i -th component depending only on c^i resp. p^i .

$(\text{prox}_t^{f_1}(c))^1$: Writing it out explicitly, one has

$$\begin{aligned} (\text{prox}_t^{f_1}(c))^1 &= \\ \argmin_{d \in \mathbb{R}^{m+2q}} &\sqrt{\sum_{i=1}^{m+2q} d_i^2 + \sum_{i=1}^{m+2q} \delta_+(d_i) + \frac{t}{2} |d_i - c_i^1|^2}. \end{aligned}$$

From this, it is apparent that any solution $\hat{d} \in \mathbb{R}^{m+2q}$ will satisfy $\hat{d}_i = 0$ if $c_i^1 \leq 0$. As such, one can replace c^1 by $[c^1]_+$

in the above minimization problem without changing the solution. But with $[c^1]_+$ instead of c^1 , it is clear that any solution of the above problem will be non-negative even without the non-negativity constraint, making it equivalent to

$$\begin{aligned} \text{prox}_t^{\lambda_p \|\cdot\|_2}([c^1]_+) = \\ \underset{d \in \mathbb{R}^{m+2q}}{\text{argmin}} \sqrt{\sum_{i=1}^{m+2q} d_i^2} + \frac{t}{2} \sum_{i=1}^{m+2q} |d_i - ([c^1]_+)_i|^2. \end{aligned}$$

By [6, Example 6.19], the solution of the latter is of the claimed form.

$(\text{prox}_t^{f_1}(c))^i$ for $i \geq 2$: Writing $f_1(c)_j^i = |c_j^i| + \delta_+(c_j^i)$ for $1 \leq j \leq N$, a combination of [6, Example 6.8] with [8, Lemma 6.14(b)] immediately yields the claimed form.

$\text{prox}_t^{f_2}(p)$: Observe that $f_2(p) = \sum_{i=1}^N \delta_{C_i}(p^i)$, where $C_i := \{x \in \mathbb{R}^{2q+1} \mid x \geq 0, \|x\|_2 \leq 1\}$. Employing [6, Theorems 6.6, 6.24 and 6.30], as well as noting that $C_i = \{x \in \mathbb{R}^{2q+1} \mid g_i(x) \leq 1\}$, where $g_i(x) := \delta_+(x) + \|x\|_2^2$ with effective domain \mathbb{R}_+^{2q+1} , one has

$$(\text{prox}_t^{f_2}(p))^i = P_{C_i}(p^i) = \begin{cases} [p^i]_+, & g_i([p^i]_+) \leq 1, \\ \text{prox}_{\lambda_{g_i}}(p^i), & \text{else,} \end{cases}$$

where $\lambda > 0$ solves

$$\begin{aligned} 1 &= g_i(\text{prox}_{\lambda_{g_i}}(p^i)) = g_i(\text{prox}_{\frac{1}{2\lambda+1}\delta_+}(\frac{p^i}{2\lambda+1})) \\ &= g_i\left(\frac{[p^i]_+}{2\lambda+1}\right) = \frac{1}{(2\lambda+1)^2} \|[p^i]_+\|_2^2, \end{aligned}$$

with the last three equalities following from [6, Theorems 6.13, 6.24 and Lemma 6.26]. Simplifying leads to the desired form. \square

3 Experiments

In this section, we provide experimental results of the proposed method for two different use cases, namely activity prediction, where we try to correctly detect whenever energy is consumed actively by a person, and multichannel disaggregation, where we aim to reconstruct all individual device signals that amount to an aggregate energy signal.

3.1 Data

For our experiments, we employ the SynD data set generator [16], an algorithm to generate synthetic energy signals.

This enables us to work with clean, yet realistic, data. The algorithm uses real device energy signatures, which it randomly alters and places throughout the day. It became apparent, however, that the fridge's energy signal generated with SynD is unrealistically regular, being identical each day; for this reason, we replaced the fridge by an energy signal taken from the UK-DALE 6 seconds data set [14], and resampled to the desired sampling rate by weighted averaging.

Explicitly, we generate two different synthetic households, referred to as *synd1* and *synd2*. Each of the two data sets consists of four devices, *synd1* of the fridge from UK-DALE's house 1 as well as SynD's electric space heater, washing machine, and hair dryer, and *synd2* of the fridge from UK-DALE's house 2 and SynD's dishwasher, iron, and water-cooker. We use a sampling rate of 1 minute, and the data sets are normalized to have values between 0 and 1.

3.2 Performance metrics

MCC score Both experiments we perform (activity prediction and multichannel disaggregation) can be cast as binary classification tasks with multiple channels. In case of activity prediction, for each time point we aim to classify the *active* signal as ON or OFF depending on whether a person is actively consuming energy or not, and similarly classify the *passive* signal as ON or OFF depending on whether a *passive device* is consuming energy or not. In case of multichannel disaggregation, for each time point we aim to classify each individual device as either ON or OFF. One should note that the proposed method, as well as all methods we compare to, yield non-binary output signals, that is, the methods predict the actively consumed energy or the individual device energy signatures, rather than a binary ON/OFF signal. In order to be able to evaluate the classification performance, these non-binary predictions are first transformed to binary signals via pointwise thresholding by 0.01 times the maximum value of the ground truth signal. That is, given $\hat{u}, u \in \mathbb{R}^m$ a true non-binary signal and its prediction (e.g., the true fridge signal and the predicted one, or the true actively consumed energy signal and the predicted one), respectively, we compute \hat{U} and U as $\hat{U} = (\hat{u} \geq 0.01 \|\hat{u}\|_\infty)$ and $U = (u \geq 0.01 \|u\|_\infty)$ in Python notation. As a metric for evaluating binary classification, we use a modified Matthews correlation coefficient (MCC). Given $\hat{U}, U \in \{0, 1\}^m$ a true binary signal and its prediction, respectively, the MCC is defined as $\text{MCC}(\hat{U}, U) :=$

$$\frac{(\text{TP})(\text{TN}) - (\text{FP})(\text{FN})}{\sqrt{(\text{TP} + \text{FP})(\text{TP} + \text{FN})(\text{TN} + \text{FP})(\text{TN} + \text{FN})}} \quad (5)$$

where $TP = \hat{U} \cdot U$, $TN = (1 - \hat{U}) \cdot (1 - U)$, $FP = (1 - \hat{U}) \cdot U$, and $FN = \hat{U} \cdot (1 - U)$, with \cdot the Euclidean scalar product, denote the number of true positives, true negatives, false positives, and false negatives, respectively. The MCC score is a value in $[-1, 1]$, where $+1$ and -1 correspond to perfect agreement or disagreement, respectively, and 0 indicates no relationship. In view of relevant monitoring applications, where it is sufficient to predict activity up to a reasonable inaccuracy in time, we introduce an *activity prediction radius* $R \in \mathbb{N}_0$ into the computation of the MCC. We first define a modified true activity \tilde{U} via

$$\tilde{U}_i = \begin{cases} 1 & \text{if } \exists j \in \{1, 2, \dots, m\}, |i - j| \leq R : \hat{U}_j = 1 \\ 0 & \text{otherwise.} \end{cases} \quad (6)$$

In other words, \tilde{U}_i is equal to one whenever there was true activity within a $(2R + 1)$ -minutes time window around the time stamp i . We then compute $TP = \tilde{U} \cdot U$, $TN = (1 - \tilde{U}) \cdot (1 - U)$, $FP = (1 - \tilde{U}) \cdot U$, and $FN = \tilde{U} \cdot (1 - U)$. Using these values, the modified MCC is obtained via (5) again and denoted as MCC_R . In our experiments, we use $R = 7$.

MSE As a second performance metric, we use the mean squared error (MSE), which is computed as $MSE(\hat{u}, u) = \frac{1}{2m} \sum_{i=1}^m (\hat{u}_i - u_i)^2$. Contrary to the MCC, which indicates whether a device/activity was predicted correctly as on/off at a certain time, the MSE instead indicates how well the shapes and magnitudes of energy signals are predicted.

3.3 Experimental setup

The CSC experiments were carried out in the following manner: Given an aggregate energy signal $u \in \mathbb{R}^m$, initialize $(c_{-1}, p_{-1}) = (c_0, p_0) \in (\mathbb{R}^{m+2q})^N \times (\mathbb{R}^{2q+1})^N$ by, e.g., selecting random non-zero features of u of appropriate length as atoms and their location, shifted appropriately, as coefficients. Pick $\alpha_1^k = \alpha_2^k = \beta_1^k = \beta_2^k = 0.7$ for all $k \in \mathbb{N}_0$, and compute the τ_1^k and τ_2^k in accordance with [23], Remark 4.1. Employ the relative change in the modified energy

$$\Psi_k := F(c_k, p_k) + \frac{\gamma_1}{2} \|c_k - c_{k-1}\|_2^2 + \frac{\gamma_2}{2} \|p_k - p_{k-1}\|_2^2$$

(c.f. [23], (4.6)) as the stopping rule; explicitly, we stop when $\frac{|\Psi_k - \Psi_{k-1}|}{\Psi_{k-1}} < 10^{-6}$ or when $\Psi_k = 0$.

3.4 Results

3.4.1 Activity prediction

In our data sets, the passive consumption is comprised solely of the fridge signal, while the active consumption consists of all remaining devices. We compare to four different methods from the non-intrusive load monitoring toolkit NILMTK [4,5], namely, combinatorial optimisation (CO), factorial hidden Markov model (FHMM), a neural network model (SEQ2SEQ) and discriminative sparse coding (DSC), the latter being conceptually similar to the proposed method. All methods are trained to predict the active and the passive energy consumption. In accordance with the design of these methods, we do not normalize the data sets before applying the methods. We do, however, normalize data and predictions before computing the performance metrics, thus ensuring a fair comparison. We report the scores on the active component of the signal in Tables 1 and 2. In Table 1, we show the testing scores for the case of training and testing on the same household. That is, all algorithms use four weeks of the energy signal for supervised training, and a different selection of four weeks of the same energy signal for testing. For the scores reported in Table 2, we trained all methods on four weeks of one data set, and tested on four weeks of the remaining data set; this serves to investigate how well the methods generalize to unseen data. Despite CSC also using data to determine parameters, we wish to stress that the method uses significantly less information for this process than the other methods. With CSC, it is not necessary to learn, e.g., the distribution of individual devices (FHMM), the shapes of device signatures (DSC), or the parameters of a neural network etc. Rather, one solely needs to determine the hyperparameters λ_a , λ_p , N and q of our energy functional. Therefore, the method is more likely to generalize well to unseen data sets. Indeed, our experiments suggest that once these parameters are fixed, the method can be applied to any comparable data set in an unsupervised fashion. Overall, in terms of quantitative results, the proposed method performs comparable to the competing methods. While SEQ2SEQ is in general advantageous in terms of MCC scores, CSC outperforms all other methods in terms of MSE scores. We believe that this relates to the fact that CSC recognizes the specific shapes of energy consumption more accurately. This is in particular supported by Figure 1. While FHMM and CO also closely fit the ground truth passive energy signal, CSC is the only method to capture the spiked shape of the fridge signal. The deficiency in the MCC score is a result of the reconstructed signal not being close enough to zero at times where the ground truth is zero. Regarding the active signal, SEQ2SEQ and CSC outperform

the remaining methods overall, both qualitatively and quantitatively, with CSC yielding the best MSE and SEQ2SEQ the best MCC scores.

	CSC	FHMM	CO	SEQ2SEQ	DSC
synd1	0.78/ 0.33	0.79/19.27	0.91/14.94	0.97 /5.95	0.44/56.58
synd2	0.95/ 0.07	0.87/5.25	0.90/4.12	0.98 /1.66	0.73/7.69

Table 1: Testing scores ($MCC_7 / MSE \times 10^4$) of the active energy usage for different methods applied to synd1 and synd2. Training and testing on different time frames of the same household. Bold indicates best result.

	CSC	FHMM	CO	SEQ2SEQ	DSC
synd1	0.63/ 0.39	0.82/6.92	0.85 /24.62	0.52/8.78	0.38/28.26
synd2	0.94 / 0.09	0.92/4.16	0.92/4.18	0.94 /3.08	0.48/19.20

Table 2: Testing scores ($MCC_7 / MSE \times 10^4$) of the active energy usage for different methods applied to synd1 resp. synd2 with training on synd2 resp. synd1. Bold indicates best result.

3.4.2 Multichannel disaggregation

In this experiment, we investigate the performance of CSC applied to multichannel disaggregation, that is, inferring all individual devices from the given aggregate energy signal. We consider again the case of estimating the parameters on a different dataset than the one used for testing. This is of particular interest, since it is not possible with any of the comparison methods. By definition, the competing methods learn characteristics of specific devices and, thus, trying to infer different devices constitutes a conceptual abuse of the method. Quantitative results can be found in Table 3, and qualitative ones in Figure 2. For inference on both synd1 and synd2, the fridge is reconstructed accurately. The reconstruction quality of active devices is more dependent on the specific device signature. We observe that devices with a more distinct and/or extended signature, such as the space heater or the iron, are reconstructed properly. The reconstruction is less precise for devices like the watercooker with a signature composed of simple peaks of a very short duration.

4 Conclusion

In this work, we developed a new method for energy disaggregation with a focus on classifying energy consumption as active or passive. This method is based on the idea of convolutional sparse coding. Our method is in principle unsupervised,

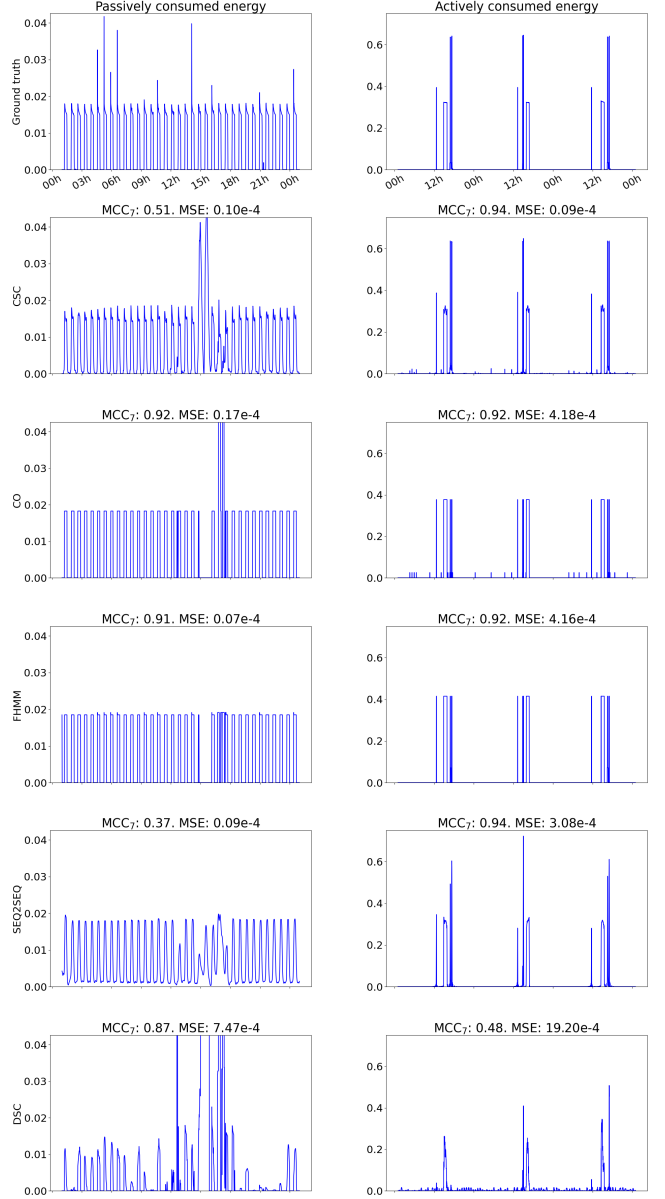
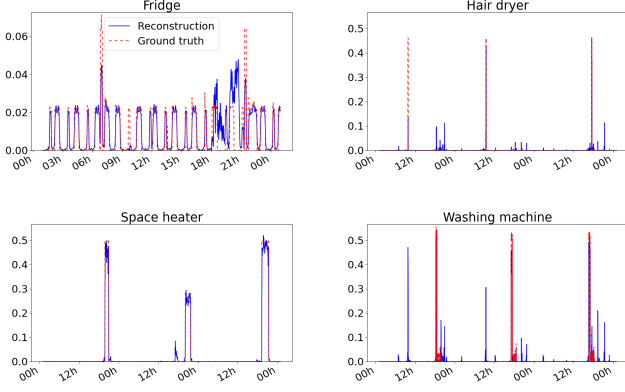


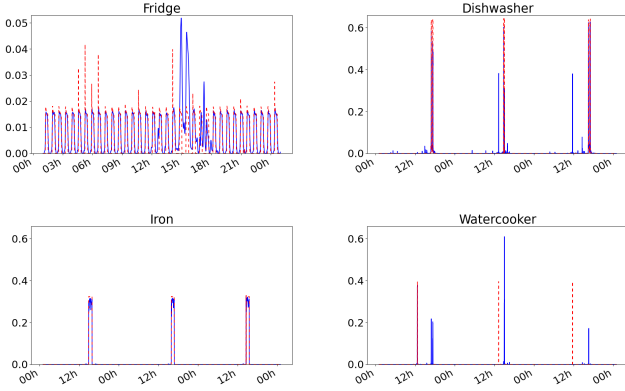
Figure 1: Predictions for active and passive energy usage with different methods. Results for inference on synd2 with training on synd1. Left column: passive energy. Right column: active energy. Top row to bottom row: ground truth, predictions with CSC, CO, FHMM, SEQ2SEQ, DSC.

synd1	Fridge	Hair dryer	Space heater	Washing machine
	0.48/0.33	0.35/2.00	0.74/1.56	0.46/3.13
synd2	Fridge	Dishwasher	Iron	Watercooker
	0.48/0.14	0.74/2.16	0.88/0.62	0.32/1.83

Table 3: Testing scores (MCC_R / $MSE \times 10^4$) of individual device signatures. Training was done on the respective other household than testing.



(a) Results on synd1



(b) Results on synd2

Figure 2: Predictions of individual devices with CSC. Results for inference with training on the respective other data set.

since we omit any prior dictionary learning. Thus, it relies only on the choice of hyperparameters, which can be fixed for a broad class of input data. We employ the iPALM algorithm for minimizing the used objective functional, which ensures strong convergence guarantees compared to many competing methods. While our unsupervised approach performs comparable to the state of the art in terms of classification scores, it yields superior performance in terms of MSE scores, recognizes specific energy consumption signatures better, and offers more flexibility due to the untrained approach. A possible future research direction is to find a heuristic for unsupervised hyperparameter fixing using, for instance, the objective functional value or the data misfit.

References

- [1] Directive (EU) 2019/944 of the European Parliament and of the Council of 5 June 2019 on common rules for the internal market for electricity and amending Directive 2012/27/EU. Online Source: eur-lex.europa.eu/legal-content/EN/ALL/?uri=CELEX%3A32019L0944, retrieved on June 23, 2022.
- [2] Intelligente Messgeräte-Einführungsverordnung. Online Source: www.ris.bka.gv.at, retrieved on May 23, 2022.
- [3] M. Aiad and P. H. Lee. Unsupervised approach for load disaggregation with devices interactions. *Energy and Buildings*, 116:96–103, 2016.
- [4] N. Batra, J. Kelly, O. Parson, H. Dutta, W. Knottenbelt, A. Rogers, A. Singh, and M. Srivastava. Nilmtk: An open source toolkit for non-intrusive load monitoring. In *Proceedings of the 5th international conference on Future energy systems*, pages 265–276, 2014.
- [5] N. Batra, R. Kukunuri, A. Pandey, R. Malakar, R. Kumar, O. Krystalakos, M. Zhong, P. Meira, and O. Parson. Towards reproducible state-of-the-art energy disaggregation. In *Proceedings of the 6th ACM international con-*

- ference on systems for energy-efficient buildings, cities, and transportation*, pages 193–202, 2019.
- [6] A. Beck. First-order methods in optimization. 2017.
- [7] J. Bolte, S. Sabach, and M. Teboulle. Proximal alternating linearized minimization for nonconvex and nonsmooth problems. *Mathematical Programming*, 146:459–494, 2014.
- [8] K. Bredies and M. Holler. Higher-order total variation approaches and generalisations. *Inverse Problems*, 36:123001, 2020.
- [9] M. Fell, H. Kennard, G. Huebner, M. Nicolson, S. Elam, and D. Shipworth. Energising health: A review of the health and care applications of smart meter data. *London, UK: SMART Energy GB*, 2017.
- [10] R. Gopinath, M. Kumar, C. P. C. Joshua, and K. Srinivas. Energy management using non-intrusive load monitoring techniques—state-of-the-art and future research directions. *Sustainable Cities and Society*, 62:102411, 2020.
- [11] G. W. Hart. Nonintrusive appliance load monitoring. *Proceedings of the IEEE*, 80(12):1870–1891, 1992.
- [12] M. J. Johnson and A. S. Willsky. Bayesian nonparametric hidden semi-markov models. 2013.
- [13] J. Kelly and W. Knottenbelt. Neural nilm: Deep neural networks applied to energy disaggregation. In *Proceedings of the 2nd ACM international conference on embedded systems for energy-efficient built environments*, pages 55–64, 2015.
- [14] J. Kelly and W. Knottenbelt. The UK-DALE dataset, domestic appliance-level electricity demand and whole-house demand from five UK homes. *Scientific Data*, 2(150007), 2015.
- [15] H. Kim, M. Marwah, M. Arlitt, G. Lyon, and J. Han. Unsupervised disaggregation of low frequency power measurements. In *Proceedings of the 2011 SIAM international conference on data mining*, pages 747–758. SIAM, 2011.
- [16] C. Klemenjak, C. Kovatsch, M. Herold, and W. Elmenreich. A synthetic energy dataset for non-intrusive load monitoring in households. *Scientific Data*, 7(1):1–17, 2020.
- [17] J. Kolter, S. Batra, and A. Ng. Energy disaggregation via discriminative sparse coding. *Advances in neural information processing systems*, 23, 2010.
- [18] J. Z. Kolter and T. Jaakkola. Approximate inference in additive factorial hmms with application to energy disaggregation. In *Artificial intelligence and statistics*, pages 1472–1482. PMLR, 2012.
- [19] A. Moradzadeh, B. Mohammadi-Ivatloo, M. Abapour, A. Anvari-Moghaddam, S. Gholami Farkoush, and S.-B. Rhee. A practical solution based on convolutional neural network for non-intrusive load monitoring. *Journal of Ambient Intelligence and Humanized Computing*, 12(10):9775–9789, 2021.
- [20] S. Pandey and G. Karypis. Structured dictionary learning for energy disaggregation. In *Proceedings of the Tenth ACM International Conference on Future Energy Systems*, pages 24–34, 2019.
- [21] S. Pattem. Unsupervised disaggregation for non-intrusive load monitoring. In *2012 11th International Conference on Machine Learning and Applications*, volume 2, pages 515–520. IEEE, 2012.
- [22] J. Paxman, M. James, E. Costanza, and J. Manning. Smart future of healthcare. *20/20health*, 2020. Online Source: 2020health.org/publication/smart-future-of-healthcare/, retrieved on June 28, 2022.
- [23] T. Pock and S. Sabach. Inertial proximal alternating linearized minimization (ipalm) for nonconvex and nonsmooth problems. *Sustainable Cities and Society*, 9:1756–1787, 2016.
- [24] S. Singh and A. Majumdar. Deep sparse coding for non-intrusive load monitoring. *IEEE Transactions on Smart Grid*, 9(5):4669–4678, 2017.
- [25] C. Zhang, M. Zhong, Z. Wang, N. Goddard, and C. Sutton. Sequence-to-point learning with neural networks for non-intrusive load monitoring. In *Proceedings of the AAAI Conference on Artificial Intelligence*, volume 32, 2018.
- [26] G. Zhou, Z. Li, M. Fu, Y. Feng, X. Wang, and C. Huang. Sequence-to-sequence load disaggregation using multi-scale residual neural network. *IEEE Transactions on Instrumentation and Measurement*, 70:1–10, 2020.